Vacuum 199 (2022) 110964

Contents lists available at ScienceDirect

Vacuum

journal homepage: www.elsevier.com/locate/vacuum

Oxygen atom density in a large reactor powered by four inductively coupled plasma sources

Gregor Primc [a,*], Dane Lojen [a,b], Alenka Vesel [a], Miran Mozetič [a], Rok Zaplotnik [a]

[a] Department of Surface Engineering, Jozef Stefan Institute, Jamova cesta 39, 1000, Ljubljana, Slovenia
[b] Jozef Stefan International Postgraduate School, Jamova cesta 39, 1000, Ljubljana, Slovenia

ARTICLE INFO

Keywords:
Inductively coupled plasma
Catalytic probe
Oxygen atoms
Industrial-size
Polymer

ABSTRACT

Gradients in O-atom density in metallic plasma reactor useful for rapid surface activation of 3D polymer products have been measured. The reactor of a volume of 150 l was equipped with four inductively coupled plasma sources (ICPS) of (predominantly) oxygen atoms, parallelly coupled with a radio-frequency generator of adjustable power up to 5 kW at 13.56 MHz. Molecular oxygen was continuously introduced into the ICP sources, where it was dissociated upon plasma conditions. The constant pumping of the plasma reactor enabled the effective transfer of O-atoms from the ICP sources, so that their density remained high in the entire chamber even far from plasma sources. The O-atom density was measured across the reactor with a movable catalytic probe calibrated for oxygen. The sophisticated immersible design enabled the O-atom density to exceed 10^{21} m^{-3} in the major chamber volume at the pressure of 20 Pa. At this pressure, a uniform plasma in the H-mode was sustained at the total real RF power of 1800 W. Significant gradients in the O-atom density were only detected next to ICP sources' exhausts and in the main chamber's metallic side tubes. Such uniform distribution of O-atoms in a large reactor is advantageous for rapid surface activation of 3D polymer products.

1. Introduction

Oxygen-plasma treatment of polymers has been a subject of numerous scientific studies due to its applicability on an industrial scale [1,2]. Such plasma is a source of charged particles, neutral reactive species, and vacuum ultraviolet (VUV) radiation [3,4]. Non-equilibrium oxygen plasma can be sustained at low pressures (often between 10 and 100 Pa) or atmospheric pressure [5,6]. Atmospheric-pressure plasmas are characterized by extensive gradients in reactive species [7,8], so they are not very useful for treating 3D objects but perform well in cases of 1D or 2D objects such as wires, foils of fabrics. Such atmospheric-pressure plasmas indeed enable treatment in continuous mode [9,10], which is preferred in the industry [10,11]. However, large gradients in plasma parameters remain an obstacle for extensive application of these plasmas for treating 3D objects, where a robot is necessary to move a plasma jet over the surface.

On the other hand, low-pressure plasmas are convenient low power density sources (power per unit volume) of neutral reactive species and thus suitable for treating objects of almost arbitrary shape [12,13]. An appropriate gaseous discharge sustains plasma, and the neutral reactive species diffuse inside the reactor, so their density may be significant even far away from plasma sources [1]. Still, gradients in O-atom density are likely to occur even in low-pressure oxygen reactors [14].

A polymer material's surface finish depends on the type of polymer and fluxes of different reactive species onto the polymer surface. The oxygen-plasma treatment usually leads to two effects: surface functionalization with polar functional groups and etching. An appropriate surface finish is achieved by optimizing fluences of different plasma species onto a polymer surface. Functionalization and etching kinetics are still a subject of extensive research. According to a recent theory [15], which has been confirmed by carefully designed experiments [16], surface functionalization with oxygen functional groups occurs in several steps. First, the hydrogen atoms on the polymer surface are substituted with hydroxyl radicals. The surface saturation with the hydroxyl groups is accomplished at the O-atom fluence as low as about 10^{19} m^{-2}. Second, epoxy bonds are formed, followed by breaking bonds between the carbon atoms in the polymer chain. Such effects have been observed at the O-atom fluence of several 10^{20} m^{-2}. The bond scission enables the formation of various functional groups and oxygen atoms' diffusion into the sub-surface film. The surface is finally saturated with polar functional groups after being treated with an O-atom fluence of about 10^{23} m^{-2}. Etching is observed simultaneously with

* Corresponding author.
E-mail address: gregor.primc@ijs.si (G. Primc).

https://doi.org/10.1016/j.vacuum.2022.110964
Received 8 December 2021; Received in revised form 11 February 2022; Accepted 17 February 2022
Available online 22 February 2022

functionalization with carboxyl or ester groups [16]. The polymers' etching rate upon treatment with oxygen atoms only may be lower than 0.1 nm/s [17]. The etching rate is usually between 1 and 10 nm/s for many polymers when exposed to weakly ionized oxygen plasma rich in oxygen atoms at room temperature [18,19]. Highly ionized oxygen plasma is not very appropriate for surface functionalization since the etching prevails and the surface wettability remains inadequate even at prolonged treatment times [20,21]. Therefore, the best conditions for surface activation of polymers are at relatively high O-atom density and low density of charged particles. The requirements are contradictory, so the careful design of a plasma reactor is necessary to meet these criteria.

The O-atom density in a plasma reactor depends on the dissociation and recombination rates. The most intensive production of oxygen atoms is in moderately ionized gaseous plasma, in particular oxygen plasma sustained by electrodeless discharges, for example, inductively coupled RF plasma [22] and microwave plasma [23]. Gas-phase recombination is unlikely to occur at pressures below about 100 Pa since a three-body collision is required. The primary loss mechanism at low pressures is heterogeneous surface recombination. The probability depends on the recombination coefficient, which depends on the type of material facing plasma and its morphology. For example, at room temperature, the recombination coefficient for oxygen atoms on stainless steel is 0.07 [24]; on glass surfaces, it is as low as 10^{-3} [25], while on extremely porous nanostructured materials, it may come close to 1 [26]. Values of O-atom loss coefficients on many polymers are a few 10^{-3}, so the polymer products inside a metallic vacuum chamber do not present a significant drain of O-atoms [27].

Stainless steel is the material of choice for the inside part of an industrial-scale low-pressure plasma reactor. However, in such reactors, it is difficult to obtain a large density of O-atoms, which is required for rapid treatment of polymeric products. Hence, using an electrodeless discharge atom source in metallic chambers is impractical. Further, a moderately large coefficient for heterogeneous surface recombination of O-atoms to parent molecules on stainless steel surfaces prevents large O-atom density at reasonable discharge power. High-power reactors are not suitable for surface activation of polymers with oxygen plasma since the surface functional groups are unstable at elevated temperatures.

The limitations of the stainless-steel reactors may be avoided by immersing electrodeless plasma sources inside the vacuum chamber, as explained in this paper.

2. Experimental details

A high-vacuum compatible stainless-steel reactor was constructed. The reactor was a cylindrical stainless-steel tube with an inner diameter of 60 cm and an inner height of 50 cm. The inner wall of the stainless-steel cylinder was overlaid with an aluminium sheet of a cylindrical shape. This sheet also had holes on the side that were aligned with side-flanges of the chamber. Aluminium is regarded as an inert material and should not represent a significant drain for oxygen atoms by heterogeneous surface recombination. The upper and bottom part of the reactor tube were terminated with 2-cm thick aluminium flanges and sealed with Viton O-rings in between. Several tubes, perpendicular to the main stainless-steel cylinder wall, were TIG-welded according to high-vacuum standards. These side-tubes served for the mounting of gauges, probes and windows. On one side, the reactor also has a door equipped with a window to reach into the chamber and get an overview of the inside. Four specifically designed dielectric tubes (or cups) were mounted onto the upper flange of the reactor as shown in Fig. 1. The dielectric tubes were placed through holes drilled into the upper flange; the vacuum-sealing was achieved with O-rings, which act as gaskets between a dielectric tube and an aluminium flange. Details of dielectric tubes can be seen on Fig. 2. In each dielectric tube there is a 3D-printed insert made of acrylonitrile butadiene styrene (ABS) that is reinforced with stainless steel rings. These 3D-printed covers serve for guidance of compressed air used for cooling of the coils and is guided from the bottom of the dielectric tube towards the top of the coils. A single RF coaxial cable from the generator (Advanced Energy, Cesar 1350) was connected to a matching network made of two vacuum capacitors, each with a capacitance between 20 and 250 pF (Commet Maxi-Con), in a gamma configuration. Forward and reflected powers were measured by the RF generator reflected power measurement functionality. Reflected

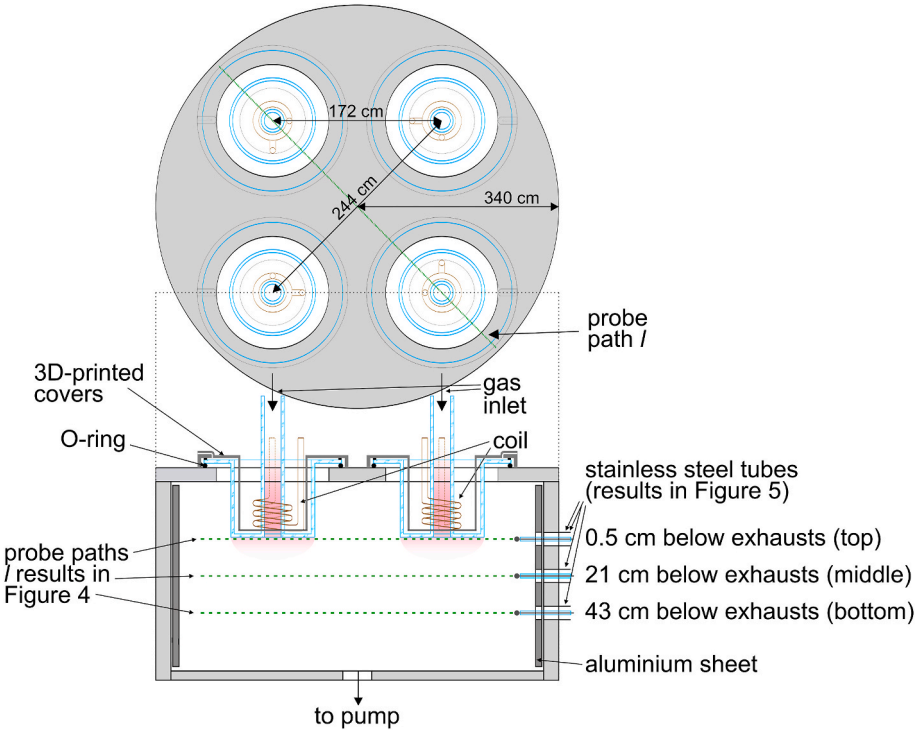

Fig. 1. Schematic of the plasma reactor (below) and the position of the four dielectric tubes for RF coils on the upper flange (above).

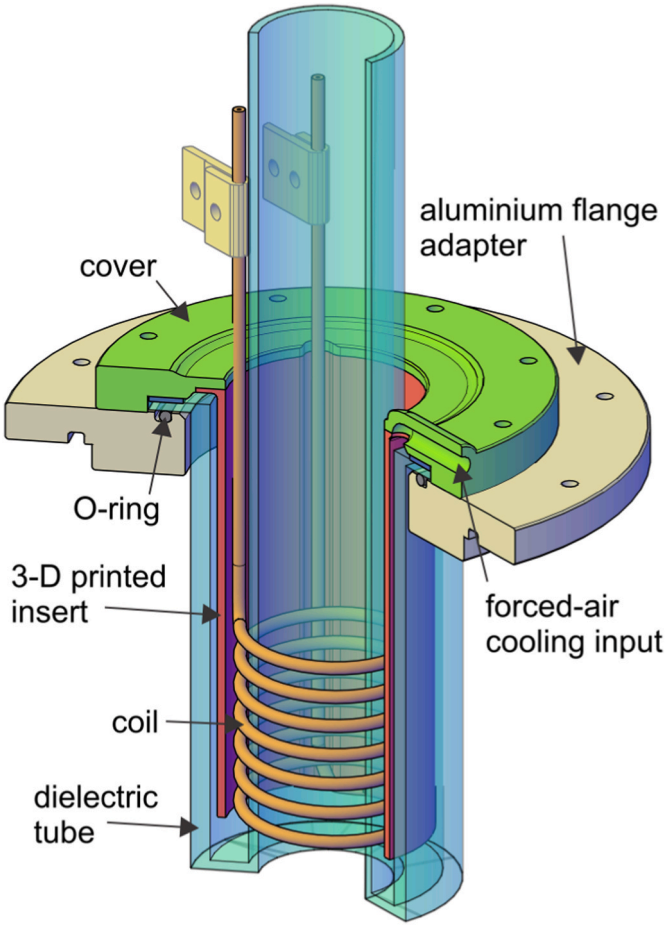

Fig. 2. Detailed schematic of a single ICP source.

power was in the range between 15 and 55 W, depending on the reactor temperature, which was gradually increasing during prolonged measurements, and daily conditions. Capacitors were always set to provide the real power of 1800 W at the start of each series of measurements. Copper coils were immersed into the dielectric tubes and connected to the matching network in parallel to ensure appropriate RF voltages on all four coils. Each coil is made from a copper tube with an outer diameter of 3 mm and inner diameter of 1 mm and has 6 and ¾ turns. Internal diameter of the coil is 42 mm. The coils were mounted on the atmospheric-pressure side, while plasma was ignited in the inner sides of dielectric tubes under vacuum conditions. The cable from the matching network was mounted on a special holder made of three 10-mm thick FR4 layers. The middle layer serves as insulation between both electrodes. The holder serves as power distributor and is made in a star-like distribution. This means that conducting paths from the RF cable to each coil are exactly the same. Moreover, between the main RF cables' hot wire and each coil (also RF cables' ground and each coil) there are sliders that are used to match any differences in the impedance for each coil. Top and bottom layers are symmetric in respect of both electrodes and can be interchangeable, meaning that the powered electrode can be on the top or bottom layer.

The reactor in Fig. 1 was pumped by a combination of roots (Busch Vacuum, Wv 0500 B OHI KAFA) and rotary (Trivac, D40B) vacuum pumps. Nominal pumping speed of the roots pump was 600 m^3/h, and the nominal ultimate pressure was about 10^{-2} Pa. The two-stage rotary pump had a nominal pumping speed of 40 m^3/h and an ultimate pressure of about 0.1 Pa. With the combination of both pumps, the plasma reactor was pumped within a few minutes down to a pressure below the detection limit of the capacitive vacuum gauge (Baratron, MKS), i.e., 1 Pa.

A catalytic probe for measuring the O-atom density was mounted on three different side tubes, as shown in Fig. 1; the distances between the end of the dielectric tubes and centers of each side tubes were 0.5, 21 and 43 cm, respectively. We used a standard probe configuration as disclosed in Ref. [28]. As depicted in Fig. 2, the thermocouple wires were embedded into a glass tube and vacuum-sealed at the end with both wires sticking outside of the glass tube. The probe was mounted to a special feedthrough that enabled continuous horizontal movement through the chamber almost without friction that would cause the outside air to protrude into the evacuated chamber. The O-ring sealing was lubricated with a high vacuum grease to assure for smooth movement of the glass tube. In short, a catalytic probe determines the O-atom density in its vicinity by measuring the heat dissipated on the surface of a small catalytic disc immersed into a gas rich in O-atoms. The oxygen atoms recombine to parent molecules on the catalytic disc's surface. The disc is thus heated well above the ambient gas temperature. The power dissipated on the disc's surface is proportional to the flux of oxygen atoms, considering the value of the recombination coefficient of the catalytic material. Cobalt was used as catalytic material since it exhibits a constant and high recombination coefficient in a broad range of temperatures and O-atom fluxes. The probe gives accurate and reliable results as long as heterogeneous surface recombination is the predominant

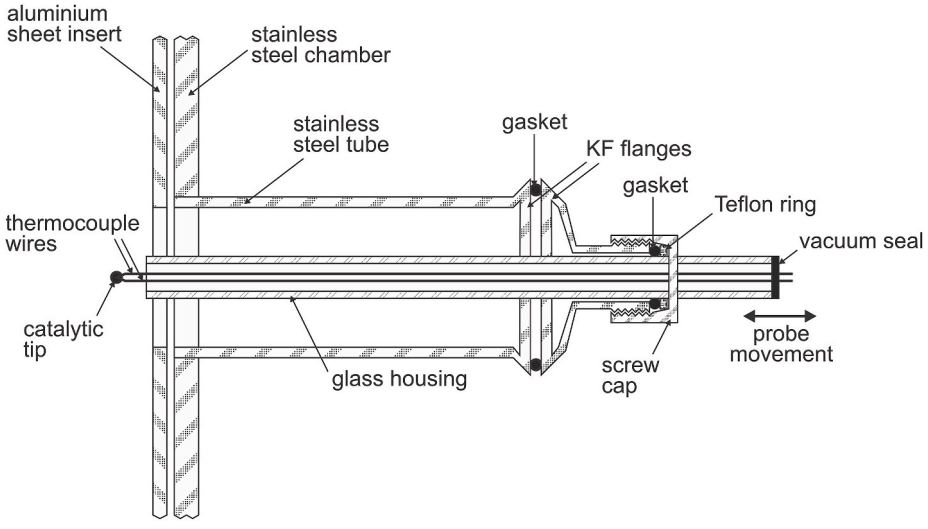

Fig. 3. Detail of the stainless-steel chamber sidewall with a movable probe.

heating mechanism, i.e., in highly dissociated weakly ionized oxygen plasmas.

The probe measurements under different conditions were compared to Ref. [29] and we found very good agreement, so the probes are regarded as a reliable tool for measuring the density of atoms in weakly ionized plasmas of molecular gases such as oxygen, nitrogen or hydrogen.

3. Results and discussion

The chamber in Fig. 1 was first evacuated to the ultimate pressure, which was below the detection limit of the capacitive vacuum gauge (1 Pa). Commercially available oxygen of purity 99.99% was leaked through a needle valve into ICP sources, as marked in Fig. 1. The plasma reactor was pumped continuously during oxygen leakage to reach the pressure of 20 Pa. Oxygen flow was 420 sccm. This pressure assured for sustaining stable plasma in the H-mode in all four ICP sources. A photo of the plasma reactor with four ICP sources at 20 Pa and the real ($P_{\text{forward}} - P_{\text{reflected}}$) RF power of 1800 W is shown in Fig. 4. The luminous plasma was concentrated within the dielectric tubes. About a centimeter below the edges of dielectric tubes, the electromagnetic field becomes too low to sustain plasma in the H-mode leading to a steep decrease in plasma emission intensity. The major volume of the plasma reactor away from the four ICP sources is therefore filled with diffusing plasma of a very weak luminosity. Such a low luminosity indicates low electron temperature and/or density in the majority of the plasma reactor. Production of oxygen atoms by dissociative collisions between plasma electrons and oxygen molecules in the plasma reactor's major volume is therefore marginal compared to the production of oxygen atoms within the ICP sources. As mentioned earlier, the gas is leaked at the top of ICP sources flowing through them into the main chamber.

The O-atom density was measured by positioning the catalytic probe through the three side tubes. The probe was movable, making it possible to determine the O-atom density along its path. The paths are indicated in Fig. 1. One port for the catalytic probe was placed just below the ICP sources, 0.5 cm below the exhausts from the dielectric tubes, as shown in Fig. 1. The second port was located in the middle of the stainless-steel cylinder and the third at the lowest position, i.e., about 3 cm from the pump duct.

The results of systematic measurements are shown in Figs. 5 and 6. In Fig. 5, the three curves represent the O-atom density at the top position (0.5 cm below dielectric tubes with RF coils), in the middle of the reactor, and at the bottom. The upper curve exhibits two maxima, while the other two curves are somewhat monotonous.

The upper curve in Fig. 5 shows an interesting probe signal along the diameter of the plasma reactor. The two maxima in the curve correspond to the position of the ICP sources. The O-atom density right below an ICP source is higher than away from the source. The effect may be explained by a higher flux of oxygen atoms at the exhaust from the ICP source. As mentioned above, the O-atom density is determined from the flux of O-atoms onto the catalytic disc surface. The flux is a product of the O-atom density (n) and the average random velocity ($<v>$), i.e., $j = ¼\, n <v>$. The random velocity increases as the square root of the gas kinetic temperature. Therefore, the maxima in the upper curve in Fig. 5 can be explained by a higher kinetic temperature of oxygen atoms next to the ICP source. The gas temperature in plasma in the H-mode is elevated due to the high density of electrons and also the super-elastic nature of the

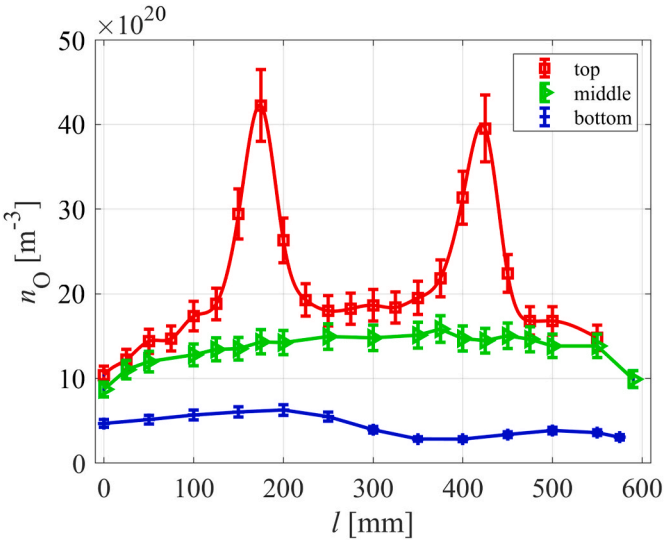

Fig. 5. The O-atom density in the plasma reactor at positions just below the ICP sources (upper curve), in the middle (middle curve), and at the bottom (lower curve) of the metallic reactor.

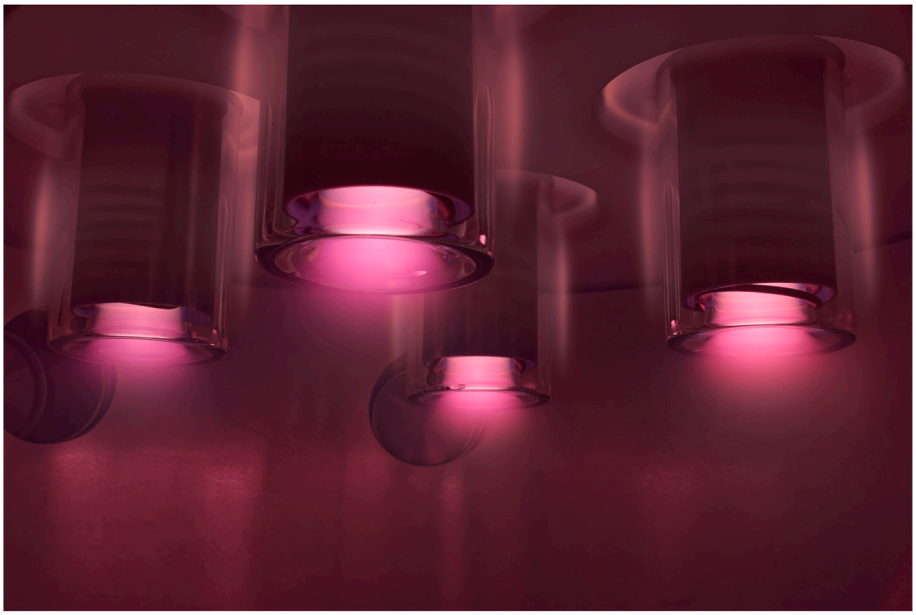

Fig. 4. A photograph of the four ICPs in the plasma reactor at 20 Pa and real power of 1800 W.

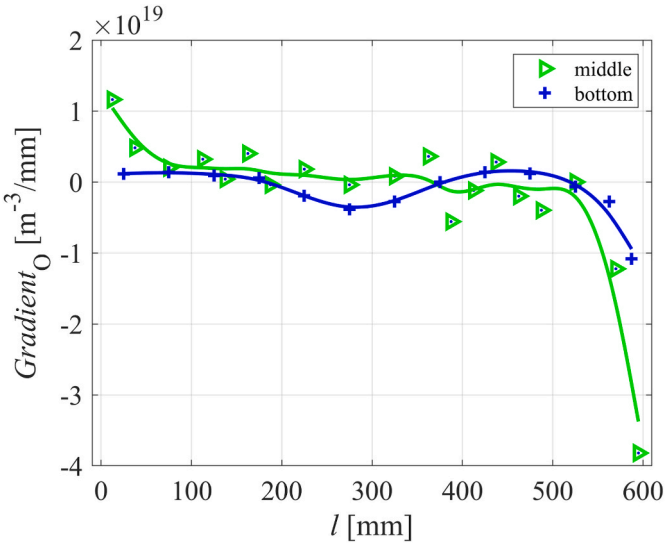

Fig. 6. Gradients of O-atom density in the middle section (21 cm from the exhausts) and at the bottom (43 cm from the exhausts).

dissociative collisions [25]. Hence these two effects may contribute to the increased probe signal when positioned just below an ICP source. Another reason for the maxima may be additional heating of the catalyst surface due to the absorption of light quanta from the ICP source. Namely, ICP plasma in the H-mode is a significant radiation source, especially in the VUV range of wavelengths [4]. The primary radiation from oxygen plasma arises from resonant transitions of oxygen atoms with peak intensity at 130.4 nm [30,31]. Whatever the reason, the O-atom density determined by the catalytic probe exhibits maxima below the ICP sources. In between ICP sources, the O-atom density is relatively constant at a value of about 2×10^{21} m^{-3}. This indicates a high dissociation fraction of O_2 molecules. Specifically, the density of oxygen molecules is $n_{O2} = p/k_B T$, where p is gas pressure, k_B Boltzmann constant, and T the neutral gas kinetic temperature. Considering the pressure is 20 Pa and temperature 300 K, the density of O_2 molecules at the selected experimental conditions with the absence of plasma is 4.8×10^{21} m^{-3}. A significant dissociation fraction of oxygen molecules (about a fifth, considering that a molecule consists of two atoms) is obtained right below ICP sources in the volume between them. The O-atom density at the exhaust of an ICP source (maxima of the upper curve in Fig. 5) is almost as high as the theoretical density of molecules at 20 Pa. However, such a high value is probably an artifact in light of the upper discussion.

The middle curve in Fig. 5 is smooth and free from maxima. The probe was moved 21 cm below the exhausts of the ICP sources when acquiring the measured points of the middle curve. The O-atom density in the middle of the reactor is almost gradient-free. The O-atom density of approx. 1.2×10^{21} m^{-3} prevails in almost the entire range of probe positions except near the reactor wall (a few centimeters away). Close to the chamber walls, gradients of O-atom density appear, which can be explained by the higher heterogeneous surface recombination value. The gradients, however, are not significant since the O-atom density at the position just next to the wall is still about 1×10^{21} m^{-3}. These small gradients appeared because the inner side of the reactor cylinder was wrapped with a thin aluminum sheet, as depicted in Figs. 1 and 3. The coefficient for heterogeneous O-atom recombination on aluminum is much smaller than on stainless steel [32].

Fig. 6 depicts spatial gradients of O-atom density in the middle (21 cm from the exhausts) and bottom section (43 cm from the exhausts). Their values were calculated as $(y_2 - y_1)/(x_2 - x_1)$, where y_1 and y_2 are the oxygen atom densities at positions x_1 and x_2. These gradients were drawn between x_1 and x_2, what basically means that each gradient point is the inclination of the line between two points between two points on the x-axis. Small gradients were also measured at the bottom of the stainless-steel reactor, where the probe was positioned 43 cm below the exhausts of ICP sources. The O-atom density versus probe position is presented as the lower curve in Fig. 5. Somehow lower O-atom density in the segment 300–600 mm compared to the segment 0–300 mm is difficult to explain. An important feature is that the density remains at around 4×10^{20} m^{-3}, although the probe was more than 40 cm away from ICP sources. The reason was already explained: selecting appropriate materials with low recombination coefficient.

As mentioned earlier, the coefficient for heterogeneous surface recombination of oxygen atoms on stainless steel surfaces is moderately high at the value of 0.07 [24]. The O-atom density within side tubes made from this material and not wrapped into an aluminum sheet should be much lower than within the main chamber. To prove this, we also performed some measurements inside a stainless-steel side tube attached to the side of the main chamber, as shown schematically in Fig. 3. A probe was moved from the main reactor wall into the stainless-steel tube. The O-atom density versus the probe's tip position in the stainless-steel side tube is presented in Fig. 7. The value $l = 0$ mm corresponds to the position of the cylindrical reactor wall and the negative values to the depth inside the stainless-steel tube. The inner diameter of the stainless-steel tube was 4 cm.

Fig. 7 reveals a strong gradient in the O-atom density inside the stainless-steel tube. The density drops for an order of magnitude in a few centimeters. The gradient is explained by heterogeneous surface recombination of the oxygen atoms on the surface of the stainless-steel tube. The tube is terminated with a KF flange which holds the catalytic probe, so any gas movement is diffusion-dependent. There is a continuous supply of oxygen atoms from the main chamber at the entrance to the stainless-steel side tube and a gradual sink on the side walls and on the flange at the end of the stainless-steel side tube. The gradient as observed in Fig. 7 is therefore expected.

The O-atom density throughout the chamber was close to 1×10^{21} m^{-3}; thus, the flux of oxygen atoms on any object placed into the reactor was a few 10^{23} m^{-2}s^{-1}. Such a large flux should ensure complete surface functionalization of commonly used polymer materials in a time below a second, making the plasma reactor effective for rapid activation of any polymer products in the continuous mode.

4. Conclusions

A high and relatively constant density of oxygen atoms can be

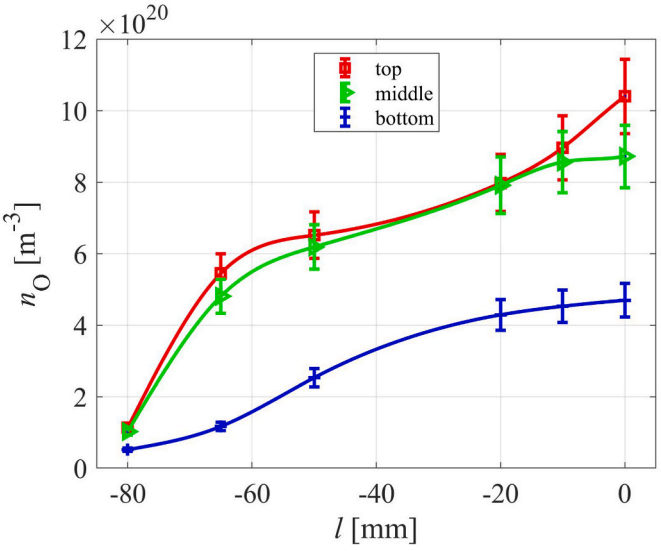

Fig. 7. The O-atom density within the side stainless steel tubes.

sustained in a large metallic plasma reactor by immersing several inductively coupled plasma sources into the reactor. The dissociation fraction of oxygen atoms in such sources is at least 40%. Continuous supply of molecular oxygen to the ICP sources and pumping the chamber enables the dissociation fraction of about 10% in the entire chamber. At our particular conditions, the dissociation fraction at the position 21 cm from the exhaust (middle) was about 25%, while at the position 43 cm from the exhaust (bottom) it was about 12%. The technique was elaborated for a cylindrical stainless-steel chamber of a diameter of 60 cm and a volume of about 150 l but is scalable to larger systems providing plasmas in the H-mode are sustained in multiple ICP sources. The experiments were performed at the oxygen pressure of 20 Pa because such a moderately low pressure ensures a relatively large gas density on the one hand and the ability to ignite the H-mode in all four ICP sources at a reasonable RF power on the other hand. Sustaining such conditions at lower pressure is trivial, but higher pressures require much higher RF power, which is not convenient for an industrial application of such sources. Both radial and longitudinal gradients of O-atom density were marginal. However, gradients in any stainless-steel side tube are relatively large due to extensive loss of atoms by heterogeneous recombination on stainless-steel surfaces. The flux of oxygen atoms on any object that might be placed in the plasma reactor is as high as a few 10^{23} $m^{-2}s^{-1}$, and it does not depend much on the position of an object. Such fluxes are suitable for processing polymers in terms of rapid functionalization, which can be achieved in under a second of plasma treatment.

CRediT authorship contribution statement

Gregor Primc: Writing – review & editing, Writing – original draft, Validation, Methodology. **Dane Lojen:** Visualization, Data curation, Formal analysis. **Alenka Vesel:** Writing – review & editing, Visualization, Investigation, Formal analysis. **Miran Mozetič:** Conceptualization, Funding acquisition, Methodology, Project administration, Writing – review & editing. **Rok Zaplotnik:** Writing – review & editing, Software, Methodology, Investigation.

Declaration of competing interest

The authors declare that they have no known competing financial interests or personal relationships that could have appeared to influence the work reported in this paper.

Acknowledgment

This research was funded by the Slovenian Research Agency, project No. L2-9235 (Innovative configuration of inductively coupled gaseous plasma sources for up-scaling to industrial-size reactors) and core funding P2-0082 (Thin-film structures and plasma surface engineering).

References

[1] F.F. Chen, Helicon discharges and sources: a review, Plasma Sources Sci. Technol. 24 (2015), 014001, https://doi.org/10.1088/0963-0252/24/1/014001.
[2] C. Arpagaus, G. Oberbossel, P. Rudolf von Rohr, Plasma treatment of polymer powders - from laboratory research to industrial application, Plasma Process. Polym. 15 (2018) 1800133, https://doi.org/10.1002/ppap.201800133.
[3] K. Niemi, D. O'Connell, N. de Oliveira, D. Joyeux, L. Nahon, J.P. Booth, T. Gans, Absolute atomic oxygen and nitrogen densities in radio-frequency driven atmospheric pressure cold plasmas: synchrotron vacuum ultra-violet high-resolution Fourier-transform absorption measurements, Appl. Phys. Lett. 103 (2013), 034102, https://doi.org/10.1063/1.4813817.
[4] U. Fantz, S. Briefi, D. Rauner, D. Wünderlich, Quantification of the VUV radiation in low pressure hydrogen and nitrogen plasmas, Plasma Sources Sci. Technol. 25 (2016), 045006, https://doi.org/10.1088/0963-0252/25/4/045006.
[5] A. Kuwabara, S. Kuroda, H. Kubota, Polymer surface treatment by atmospheric pressure low temperature surface discharge plasma: its characteristics and comparison with low pressure oxygen plasma treatment, Plasma Sci. Technol. 9 (2007) 181–189, https://doi.org/10.1088/1009-0630/9/2/14.
[6] X. Lu, D. Liu, Y. Xian, L. Nie, Y. Cao, G. He, Cold atmospheric-pressure air plasma jet: physics and opportunities, Phys. Plasmas 28 (2021) 100501, https://doi.org/10.1063/5.0067478.
[7] J. Dedrick, S. Schröter, K. Niemi, A. Wijaikhum, E. Wagenaars, N. de Oliveira, L. Nahon, J.P. Booth, D. O'Connell, T. Gans, Controlled production of atomic oxygen and nitrogen in a pulsed radio-frequency atmospheric-pressure plasma, J. Phys. D Appl. Phys. 50 (2017) 455204, https://doi.org/10.1088/1361-6463/aa8da2.
[8] A. Mai-Prochnow, R. Zhou, T. Zhang, K. (Ken) Ostrikov, S. Mugunthan, S.A. Rice, P. J. Cullen, Interactions of plasma-activated water with biofilms: inactivation, dispersal effects and mechanisms of action, Npj Biofilm. Microb. 7 (2021) 11, https://doi.org/10.1038/s41522-020-00180-6.
[9] K. O'Flynn, V. Milosavljević, P. Dobbyn, D.P. Dowling, Evaluation of a reel-to-reel atmospheric plasma system for the treatment of polymers, Surface. Interfac. 6 (2017) 162–169, https://doi.org/10.1016/j.surfin.2017.01.005.
[10] X. Yu, W. Chao-Liang, Q. Si-Cheng, Z. Yu, H. Tao, G. Ying, D. Ke, Z. Yu-Ru, Y. Wei, S. Jian-Jun, D. Cheng-Ran, Z. Jing, Treatment uniformity of atmospheric pressure plasma on flexible and porous material surface: a critical review, Acta Phys. Sin. 70 (2021), https://doi.org/10.7498/aps.70.20210077, 099401–099401.
[11] J. Heine, R. Damm, C. Gerhard, S. Wieneke, W. Viöl, Surface activation of plane and curved automotive polymer surfaces by using a fittable multi-pin DBD plasma source, Plasma Sci. Technol. 16 (2014) 593–597, https://doi.org/10.1088/1009-0630/16/6/10.
[12] P. Ahr, T. V Tsankov, J. Kuhfeld, U. Czarnetzki, Inductively coupled array (INCA) discharge, Plasma Sources Sci. Technol. 27 (2018) 105010, https://doi.org/10.1088/1361-6595/aadb69.
[13] M. Evrard, A. Besnard, S. Lucas, Study of the influence of the pressure and rotational motion of 3D substrates processed by magnetron sputtering: a comparative study between Monte Carlo modelling and experiments, Surf. Coating. Technol. 378 (2019) 125070, https://doi.org/10.1016/j.surfcoat.2019.125070.
[14] K. Kutasi, V. Guerra, P.A. Sá, Active species downstream of an Ar–O 2 surface-wave microwave discharge for biomedicine, surface treatment and nanostructuring, Plasma Sources Sci. Technol. 20 (2011), 035006, https://doi.org/10.1088/0963-0252/20/3/035006.
[15] R.C. Longo, A. Ranjan, P.L.G. Ventzek, Density functional theory study of oxygen adsorption on polymer surfaces for atomic-layer etching: implications for semiconductor device fabrication, ACS Appl. Nano Mater. 3 (2020) 5189–5202, https://doi.org/10.1021/acsanm.0c00618.
[16] A. Vesel, R. Zaplotnik, M. Mozetič, G. Primc, Surface modification of PS polymer by oxygen-atom treatment from remote plasma: initial kinetics of functional groups formation, Appl. Surf. Sci. 561 (2021) 150058, https://doi.org/10.1016/j.apsusc.2021.150058.
[17] A. Vesel, M. Kolar, A. Doliska, K. Stana-Kleinschek, M. Mozetic, Etching of polyethylene terephthalate thin films by neutral oxygen atoms in the late flowing afterglow of oxygen plasma, Surf. Interface Anal. 44 (2012) 1565–1571, https://doi.org/10.1002/sia.5064.
[18] L.P.T. Schepers, W.L. IJzerman, J. Beckers, Oxygen content dependent etch rate of single polymer microparticles confined in the sheath region of a low pressure radiofrequency argon/oxygen plasma, J. Phys. D Appl. Phys. 51 (2018) 375203, https://doi.org/10.1088/1361-6463/aad5b4.
[19] S. Saloum, S. Abou Shaker, M. Alwazzeh, R. Hussin, Polymer surface modification using He/O 2 RF remote low-pressure plasma, Surf. Interface Anal. 53 (2021) 754–761, https://doi.org/10.1002/sia.6976.
[20] Y. Setsuhara, K. Cho, K. Takenaka, A. Ebe, M. Shiratani, M. Sekine, M. Hori, E. Ikenaga, H. Kondo, O. Nakatsuka, S. Zaima, Plasma surface treatment of polymers with inductivity-coupled RF plasmas driven by low-inductance antenna units, Thin Solid Films 518 (2009) 1006–1011, https://doi.org/10.1016/j.tsf.2009.07.161.
[21] T. Shinozuka, T. Kawakami, H. Okamura, M. Tsunooka, M. Shirai, Methacrylonitrile based Si-containing polymers for 157-nm positive resist, J. Photopolym. Sci. Technol. 15 (2002) 629–636, https://doi.org/10.2494/photopolymer.15.629.
[22] A. Annušová, D. Marinov, J.-P. Booth, N. Sirse, M.L. da Silva, B. Lopez, V. Guerra, Kinetics of highly vibrationally excited O 2 (X) molecules in inductively-coupled oxygen plasmas, Plasma Sources Sci. Technol. 27 (2018), 045006, https://doi.org/10.1088/1361-6595/aab47d.
[23] P. Vašina, V. Kudrle, A. Tálský, P. Boto, M. Mrázková, M. Meško, Simultaneous measurement of N and O densities in plasma afterglow by means of NO titration, Plasma Sources Sci. Technol. 13 (2004) 668–674, https://doi.org/10.1088/0963-0252/13/4/016.
[24] M. Mozetič, A. Zalar, Recombination of neutral oxygen atoms on stainless steel surface, Appl. Surf. Sci. 158 (2000) 263–267, https://doi.org/10.1016/S0169-4332(00)00007-6.
[25] J.P. Booth, O. Guaitella, A. Chatterjee, C. Drag, V. Guerra, D. Lopaev, S. Zyryanov, T. Rakhimova, D. Voloshin, Y. Mankelevich, Oxygen (3 P) atom recombination on a Pyrex surface in an O 2 plasma, Plasma Sources Sci. Technol. 28 (2019), 055005, https://doi.org/10.1088/1361-6595/ab13e8.
[26] M. Mozetic, A. Vesel, S.D. Stoica, S. Vizireanu, G. Dinescu, R. Zaplotnik, Oxygen atom loss coefficient of carbon nanowalls, Appl. Surf. Sci. 333 (2015) 207–213, https://doi.org/10.1016/j.apsusc.2015.02.020.
[27] J. Krištof, P. Macko, P. Veis, Surface loss probability of atomic oxygen, Vacuum 86 (2012) 614–619, https://doi.org/10.1016/j.vacuum.2011.07.041.
[28] I. Šorli, R. Ročak, Determination of atomic oxygen density with a nickel catalytic probe, J. Vac. Sci. Technol. A Vac. Surf. Film 18 (2000) 338, https://doi.org/10.1116/1.582189.

[29] F. Gaboriau, U. Cvelbar, M. Mozetic, A. Erradi, B. Rouffet, Comparison of TALIF and catalytic probes for the determination of nitrogen atom density in a nitrogen plasma afterglow, J. Phys. D Appl. Phys. 42 (2009), 055204, https://doi.org/10.1088/0022-3727/42/5/055204.
[30] J. Lee, D.B. Graves, The effect of VUV radiation from Ar/O2 plasmas on low-k SiOCH films, J. Phys. D Appl. Phys. 44 (2011) 325203.
[31] J.R. Woodworth, M.E. Riley, V.A. Amatucci, T.W. Hamilton, B.P. Aragon, Absolute intensities of the vacuum ultraviolet spectra in oxide etch plasma processing discharges, J. Vac. Sci. Technol. A Vac. Surf. Film 19 (2001) 45–55, https://doi.org/10.1116/1.1335685.
[32] S. Wickramanayaka, S. Meikle, T. Kobayashi, N. Hosokawa, Y. Hatanaka, Measurements of catalytic efficiency of surfaces for the removal of atomic oxygen using NO * 2 continuum, J. Vac. Sci. Technol. A Vac. Surf. Film 9 (1991) 2999–3002, https://doi.org/10.1116/1.577163.